Applied Mathematics and Computation 324 (2018) 239–253

Contents lists available at ScienceDirect

Applied Mathematics and Computation

journal homepage: www.elsevier.com/locate/amc

Non-uniform interpolatory subdivision surface

Xin Li*, Yubo Chang

University of Science and Technology of China, Hefei, Anhui, PR China

ARTICLE INFO

Keywords:
Subdivision
Interpolatory subdivision
Centripetal parametrization
Chordal parametrization

ABSTRACT

This paper presents an interpolatory subdivision scheme with non-uniform parametrization for arbitrary polygon meshes with arbitrary manifold topology. This is the first attempt to generalize the non-uniform four point interpolatory curve subdivision to surface with extraordinary points. The scheme is constructed from the inspiration of the relation between the non-uniform four-point interpolatory subdivision scheme and the non-uniform B-spline refinement rule. Numerical examples and comparisons with the uniform interpolatory subdivision schemes indicate that the quality of the limit surface can be improved by using non-uniform parameter values for non-uniform initial data.

1. Introduction

Subdivision algorithm is a generalization of the spline representation to define arbitrary topology free-form surfaces [1]. Given a sequence of vertices, subdivision is a process that adds new vertices as linear combinations of old ones and meanwhile keeps or changes the positions of old vertices in each refinement step. Repeating this process leads to a limit subdivision curve or surface. A subdivision scheme is classified into an approximating one or an interpolatory one depending on whether the old vertices move or not during each refinement step. Many subdivision schemes developed from splines are usually approximating, such as Doo–Sabin subdivision [2], Catmull–Clark subdivision [3], Loop subdivision [4], $\sqrt{3}$-subdivision [5], 4–8 subdivision [6,7], Quad/triangle subdivision [8,9]. The first significant publication for interpolatory subdivision scheme is defined in [10], that introduces four-point curve subdivision scheme. And later a set of interpolatory subdivision schemes are constructed, such as Butterfly scheme [11,12], interpolatory subdivision for quadrilateral nets [13,14], interpolatory $\sqrt{3}$ and $\sqrt{2}$ subdivision [15,16]. Some interpolatory subdivision schemes are derived from approximating ones, such as the schemes from Catmull–Clark subdivision [17–21], the schemes from univariate splines [22–26], and the schemes from box splines [27–29]. Another method for interpolation is to construct a new control grid such that the limit surface of an approximating subdivision interpolates the given control grid, such as [30–32] for the Catmull–Clark surface and [33–35] for the Doo–Sabin surface. In order to construct the NURBS-compatible subdivision scheme, several non-uniform approximating subdivision schemes are constructed in [36–43].

Parametric interpolation is widely used in computer graphics and computer-aided design in many applications. In the spline curve interpolation, the choice of the knots makes a great deal of difference in the resulting curve [44]. The curve generated from uniform parameterization is generally unsatisfactory, which can be improved by properly choosing the parametrization [44,45]. In the context of interpolatory subdivision curve with non-uniform parametrizations, it is firstly introduced in [46]. And recently, the scheme is applied to reduce the undesired undulations in [47–49]. However, no literature

* Corresponding author.
E-mail address: lixustc@ustc.edu.cn (X. Li).

https://doi.org/10.1016/j.amc.2017.11.035
0096-3003/

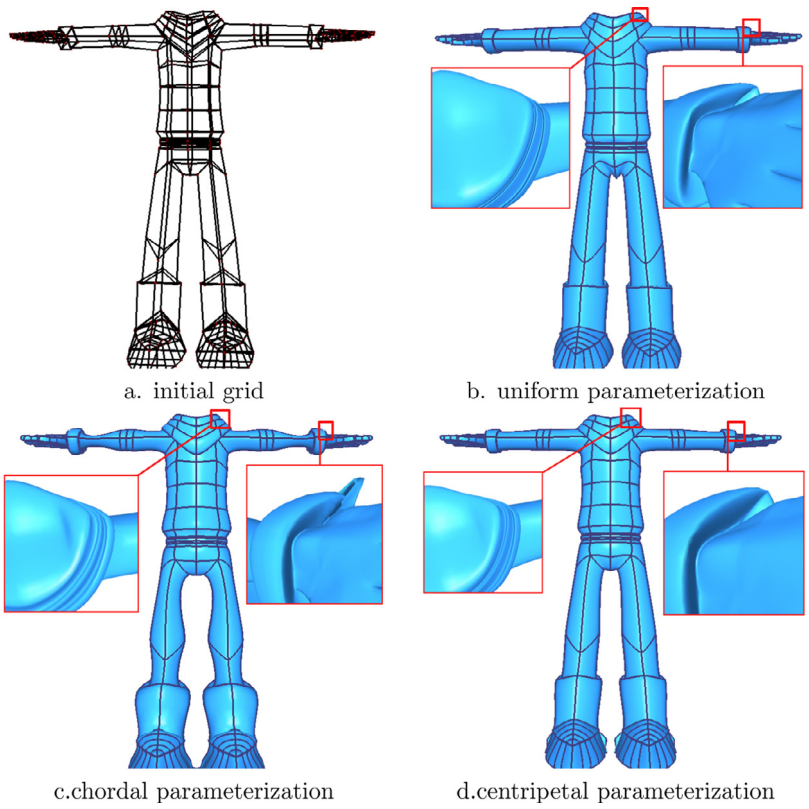

Fig. 1. Subdivision surface with different parametrization methods. Figure (a) is the initial control grid, figures (b), (c), and (d) are the interpolation subdivision surfaces with uniform, chordal and centripetal parametrization.

generalizes the non-uniform interpolatory subdivision curve scheme to surface except [50], which proposes an interpolatory subdivision surface scheme for a tensor-product control grid with a non-uniform, non-tensor-product parameterization.

In this paper, we present an interpolatory subdivision surface scheme for arbitrary manifold topological polygon meshes with the non-uniform parametrization by assigning a positive knot interval to each edge. The subdivision scheme is constructed from a relation between the non-uniform four-point subdivision scheme and the non-uniform B-spline refinement rule. The non-uniform option makes the scheme comparable to the NURBS industrial-standard and has more freedoms to adjust the shape. We will refer to them collectively as Non-Uniform Interpolatory Subdivision Surfaces (NUISSes). NUISSes include the following basic features.

- NUISSes can handle arbitrary topological meshes with arbitrary positive knot intervals, i.e., the knot intervals for the opposite edges of a face can be different;
- The limit surface of NUISS scheme is globally C^1 continuity except at the extraordinary points which continuity is verified to be G^1 with some numerical experimentations.
- If all the knot intervals are the same, then the scheme produces the interpolatory subdivision scheme in [20];
- If the mesh has no extraordinary points, all the faces are quadrilaterals, and the knot intervals for the opposite edges of any face are the same, then the scheme is reduced to the non-uniform tensor-product four-point subdivision scheme.

The performance of using NUISSes for non-uniform initial data yields better limit surfaces than those of using uniform ones. Fig. 1 shows one simple example with different parametrization (see Section 2 for the definition of uniform, chordal and centripetal parameterizations). The plots confirm the well-known effect that the uniform parametrization tends to give surfaces that are very tight to long edges and overshoot to short ones, often leads to unwanted cusps and loops, such as the self-intersections in Fig. 1b. On the other hand, the chordal parametrization scheme leads to very roundish shapes for the short edges and has relatively large distance to the long ones and may introduce self-intersections for the very short edges, such as the behavior in Fig. 1c. The limit surfaces with centripetal parametrization nicely mediate between these two extremes (Fig. 1d). Similar effects are known for interpolatory curve subdivision scheme and spline interpolation with uniform, chordal and centripetal parametrizations. The rest of the paper is organized as follows. In Section 2, we review the non-uniform four-point interpolatory subdivision curve scheme and the basic notations to define a non-uniform interpolatory subdivision surface scheme. In Section 3, we firstly give a relation between non-uniform four-point interpolatory subdivision scheme and non-uniform B-spline refinement rule. And then we provide a new framework to construct non-uniform

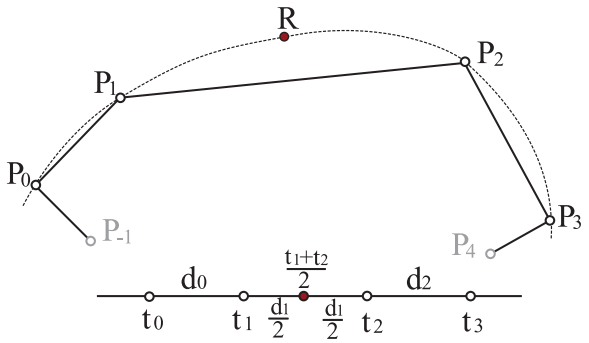

Fig. 2. Non-uniform four-point interpolatory subdivision scheme.

interpolatory subdivision surface scheme based on the relation. The detailed NUISS scheme is constructed in Section 4. In Section 5, we show some significant examples confirming the effectiveness of our interpolatory subdivision algorithms when they are applied to non-uniform data. A comparison with the limit surfaces obtained through with different parametrization will also be presented in this section. The last section gives the conclusions and future work.

2. Non-uniform interpolatory curve and surface subdivision scheme

The subdivision scheme we aim to define is conceived as a generalization of a univariate, non-uniform interpolatory four-point scheme [46–49]. Therefore, before defining the surface scheme, we first review the univariate one. Referring to Fig. 2, we are considering four consecutive points P_i with associated parameters t_i. Denote $d_i = t_{i+1} - t_i$, which is assigned to edge P_iP_{i+1} geometrically. The non-uniform four-point interpolatory subdivision computes a new point R as the linear combination of the four points P_i with ϕ_i,

$$R = \sum_{i=0}^{3} P_i \phi_i(d_0, d_1, d_2). \tag{1}$$

Here ϕ_i are called *cardinal basis functions* which are globally C^1 and can represent the quadratic or cubic polynomial in general.

In the present paper, we are using the non-uniform quadratic fundamental splines to compute ϕ_i [48],

$$R = -\frac{d_1^2}{8d_0(d_0+d_1)}P_0 + \left(\frac{d_1(d_1+d_2-d_0)}{8d_0(d_1+d_2)} + \frac{1}{2}\right)P_1 + \left(\frac{d_1(d_1+d_0-d_2)}{8d_2(d_1+d_0)} + \frac{1}{2}\right)P_2 - \frac{d_1^2}{8d_2(d_2+d_1)}P_3,$$

Now, we can consider the surface case. Let $\mathbf{M}^0$ be a regular manifold grid and P_i^0 be the vertices of $\mathbf{M}^0$. We associate each edge $P_i^0P_j^0$ with a knot interval. The knot intervals can be either specified by the user or can be computed from the mesh geometry. Precisely, the edge with two end points P_i^0 and P_j^0 can be assigned with a knot interval $||P_i^0 - P_j^0||^\alpha$, where $\alpha = 1$ gives chordal parameterization and $\alpha = \frac{1}{2}$ gives centripetal parameterization. Noted that $\alpha = 0$ corresponds to uniform parameterization. A non-uniform interpolatory subdivision surface can be considered as an iterative procedure that takes the mesh $\mathbf{M}^k$ as input with the associated knot intervals and generates a new mesh surface $\mathbf{M}^{k+1}$ with the new knot intervals based on the steps outlined below.

1. Compute a new face point (rectangle control points in Fig. 3a) for each face;
2. Compute a new edge point (solid circle control points in Fig. 3a) for each edge;
3. Construct the new mesh $\mathbf{M}^{k+1}$:
   - Create new edges by connecting each new face point to the new edge points of the edges surrounding the face, and connecting each vertex to the new edge points of the edges incident on that vertex;
   - Create new faces that have a loop of four new edges;
   - Compute the knot intervals for $\mathbf{M}^{k+1}$ as shown in Fig. 3b: the knot intervals defined in correspondence to edges of the coarse mesh are halved and duplicated, while those in correspondence to a new edge created inside a face are obtained by averaging knot intervals on the opposite new edges of the refined face. (Fig. 4)

We can see that the key step for the non-uniform interpolatory subdivision surface scheme is to define the face and edge points rules. For the points which are not in the one neighbor of the extraordinary points, the edge points can be constructed using the univariate, non-uniform interpolatory four-point scheme and the face points can be defined using the tensor-product of non-uniform interpolatory four-point scheme with the average parameterization [50]. However, for those edge and face points in the one neighbor of the extraordinary points (the points inside the grey region of Fig. 3a), there is no natural way to generalize the univariate non-uniform interpolatory four-point scheme to surface with extraordinary points.

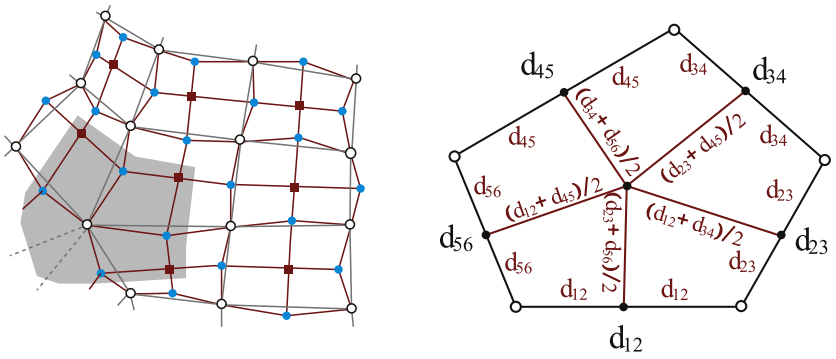

a. face and edge points b. new knots

Fig. 3. The framework of construction interpolatory subdivision surface scheme.

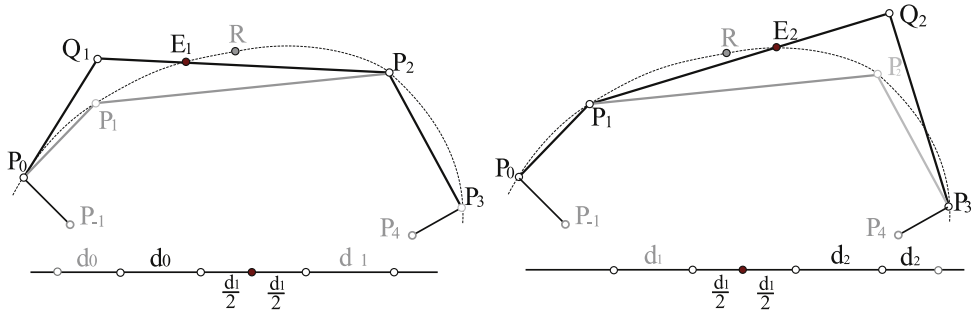

(a) Compute the temporary point E_1. (b) Compute the temporary point E_2.

Fig. 4. The relation between non-uniform four-point interpolatory subdivision curve scheme and cubic B-spline refinement rule.

3. An new approach for non-uniform interpolatory subdivision surface

The goal of this section is to provide a general formulation of a non-uniform interpolatory subdivision scheme for arbitrary topological meshes. The key idea is from the observation of the non-uniform curve interpolation subdivision rule can be derived from non-uniform B-spline refinement rules, i.e., the rule to compute R in the last section can also be derived by non-uniform cubic B-spline knot insertion algorithm as follows. (Fig. 4)

- Compute a temporary edge point E_1 by the following two steps.
  1. Compute Q_1 via Eq. (2),

$$Q_1 = \frac{(2d_0+d_1)(d_0+2d_1)}{6d_0d_1}P_1 - \frac{d_1(d_0+2d_1)}{6d_0(d_0+d_1)}P_0 - \frac{d_0(2d_0+d_1)}{6d_1(d_0+d_1)}P_2. \tag{2}$$

  Here the geometric meaning of Q_1 is that the image of the non-uniform B-spline curve with control points P_{-1}, P_0, Q_1, P_2, P_3 and the associated temporary knot intervals d_0, d_0, d_1, d_1 at $\frac{t_1+t_2}{2}$ is P_1.
  2. E_1 is the edge point for edge Q_1P_2 by non-uniform B-spline knot insertion algorithm,

$$E_1 = \frac{3d_1}{2d_0+4d_1}Q_1 + \frac{2d_0+d_1}{2d_0+4d_1}P_2 = \frac{2d_0+d_1}{4(d_0+d_1)}P_2 + \frac{2d_0+d_1}{4d_0}P_1 - \frac{d_1^2}{4d_0(d_0+d_1)}P_0.$$

- Compute a temporary edge point E_2 similarly.
  1. Compute Q_2 via Eq. (3),

$$Q_2 = \frac{(2d_2+d_1)(d_2+2d_1)}{6d_2d_1}P_2 - \frac{d_1(d_2+2d_1)}{6d_2(d_2+d_1)}P_3 - \frac{d_2(2d_2+d_1)}{6d_1(d_2+d_1)}P_1. \tag{3}$$

  Here the geometric meaning of Q_2 is that the image of the non-uniform B-spline curve with control points P_0, P_1, Q_2, P_3, P_4 and the associated temporary knot intervals d_1, d_1, d_2, d_2 at $\frac{t_1+t_2}{2}$ is P_2.
  2. E_2 is the edge point for edge Q_2P_2 by non-uniform B-spline knot insertion algorithm,

$$E_2 = \frac{3d_1}{2d_2+4d_1}Q_2 + \frac{2d_2+d_1}{2d_2+4d_1}P_1 = \frac{2d_2+d_1}{4(d_2+d_1)}P_1 + \frac{2d_2+d_1}{4d_2}P_2 - \frac{d_1^2}{4d_2(d_2+d_1)}P_3.$$

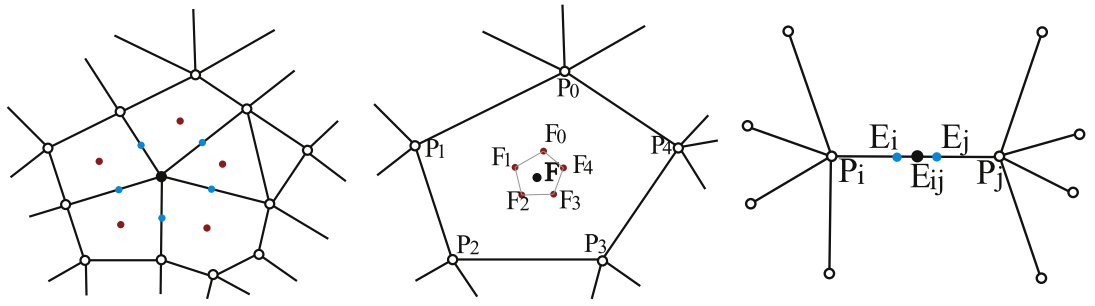

(a) Compute the contribution for each vertex. (b) Compute the face points. (c) Compute the edge points.

Fig. 5. The main processes of the new interpolatory scheme.

- It is easy to see that R is the average of the two temporary edge points E_1 and E_2.

If we denote

$$\varphi_0(d_0,d_1,d_2) = -\frac{d_1^2}{4d_0(d_0+d_1)}, \qquad \varphi_1(d_0,d_1,d_2) = \frac{2d_0+d_1}{4d_0},$$
$$\varphi_2(d_0,d_1,d_2) = \frac{2d_0+d_1}{4(d_0+d_1)}, \qquad \varphi_3(d_0,d_1,d_2) = 0,$$

then the above observation actually leads to the following equations,

$$\phi_i(d_0,d_1,d_2) = \frac{\varphi_i(d_0,d_1,d_2)+\varphi_{3-i}(d_2,d_1,d_0)}{2}, i = 0,\ldots,3. \tag{4}$$

We can use the above observation to generalize the idea to surface case, i.e., the non-uniform interpolatory surface subdivision scheme can be defined from a non-uniform approximating subdivision scheme through the following basic framework. The basic requirements for the non-uniform approximating subdivision are the *face point rule*, *edge point rule* and *the rule to compute the limit point for a vertex*. Referring to Fig. 5.

1. Compute a temporary control point for each vertex such that the limit position of the grid with the temporary points is identical to the vertex;
2. Compute the contributions for the neighbor edge points and face points according to the edge and face points rules of an approximating subdivision scheme with the temporary point.
3. Compute the real face points and edge points for the interpolatory subdivision scheme as the average of all the contributions.

4. Interpolatory subdivision surface with non-uniform parametrization

In this section, we define the NUISS rules such that they specialize the uniform interpolatory subdivision scheme [20] when all the knot intervals are the same and the tensor-product of non-uniform four-point interpolatory subdivision scheme if the mesh has no extraordinary points.

4.1. Limit point rules

The first step is to define a limit point rule such that it will produce the non-uniform B-spline rule for the regular points and it will produce Catmull–Clark rule for the extraordinary points when all the knot intervals are the same.

Suppose we are given a valence n vertex P_0 with n neighbor vertices $P_i, i = 1,\ldots,n$ and n other vertices $P_{i+n}, i = 1,\ldots,n$ for the n adjacent faces. Denote the knot intervals for edge P_0P_i are $d_{0,i}$ for $i = 1,\ldots,n$. The other knot intervals are illustrated in Fig. 6. Then the limit point C can be written as the linear combination of P_i and P_{i+n} with the coefficients as

$$C = \left(1 - \sum_{i=1}^{n}(m_i + f_i)\right)P_0 + \sum_{i=1}^{n}(m_iP_i + f_iP_{i+n}),$$

here m_i, f_i are functions of knot intervals $d_{0,i}$. Referring to Fig. 6, if all the knot intervals $d_{0,i}$ are same, then $m_i = \frac{4}{n(n+5)}$

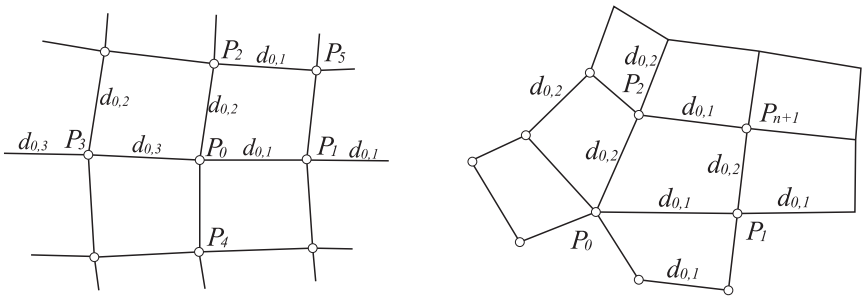

a. valence 4 b. extraordinary points

Fig. 6. Define the limit point rule.

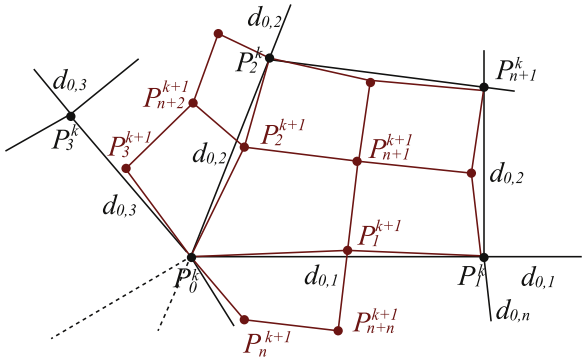

Fig. 7. Compute the contributions for the neighbor edge points and face points according to approximating subdivision scheme for a valence n vertex.

and $f_i = \frac{1}{n(n+5)}$. And if $n = 4$, m_i and f_i can be computed via B-spline knot insertion. Here we only give the equations for m_1 and f_1. The other equations are similar.

$$m_1 = \frac{d_{0,3}d_{0,4}}{\sum_{i=1}^{4} d_{0,i}d_{0,i+1}} \frac{2d_{0,2}d_{0,3}}{(2d_{0,2}+d_{0,4})(2d_{0,1}+d_{0,3})} + \frac{d_{0,2}d_{0,3}}{\sum_{i=1}^{4} d_{0,i}d_{0,i+1}} \frac{2d_{0,4}d_{0,3}}{(d_{0,2}+2d_{0,4})(2d_{0,1}+d_{0,3})};$$

$$f_1 = \frac{d_{0,3}d_{0,4}}{\sum_{i=1}^{4} d_{0,i}d_{0,i+1}} \frac{d_{0,1}d_{0,2}}{(2d_{0,2}+d_{0,4})(2d_{0,1}+d_{0,3})}.$$

Thus, m_i, f_i can be defined by combining these two cases. We can see that there are many choices to choose the m_i and f_i. In the present paper, we only choose a simple rule to define m_i and f_i.

$$m_i = \frac{9}{n+5} \frac{4(d_{0,i-2}+d_{0,i+2})}{4d_{0,i}+d_{0,i-2}+d_{0,i+2}} \left(c_i \frac{d_{0,i+1}}{4d_{0,i+1}+d_{0,i-1}+d_{0,i+3}} + c_{i-1} \frac{d_{0,i-1}}{4d_{0,i-1}+d_{0,i-3}+d_{0,i+1}} \right);$$

and

$$f_i = \frac{9}{n+5} c_i \frac{(d_{0,i-2}+d_{0,i+2})(d_{0,i-1}+d_{0,i+3})}{(4d_{0,i}+d_{0,i-2}+d_{0,i+2})(4d_{0,i+1}+d_{0,i-1}+d_{0,i+3})},$$

where $c_i = \frac{\prod_{j=i+2}^{n+i-1} d_{0,j}}{\sum_{j=1}^{n} \prod_{j=i+2}^{n+i-1} d_{0,j}}$

4.2. Non-uniform interpolatory subdivision rules

Now we are ready to define the NUISS scheme with the help of the observation in Section 3, the limit point rule in Section 4.1 and the edge, face point rules defined in [36]. In order to make the notations simple, we only define the rules for a quadrilateral mesh. But the approach can be easily extended to arbitrary polygon meshes.

Referring to Fig. 7, we denote the n adjacent vertices by P_i^k, the other vertices of the ith face by P_{i+n}^k and the knot intervals are $d_{0,i}$ for $i = 1, 2, \ldots, n$. Then we need to compute the contribution for a valence n vertex P_0^k to the neighbor face points P_{i+n}^{k+1} and edge points P_i^{k+1}. The geometric rules for the contributions are listed via the following steps.

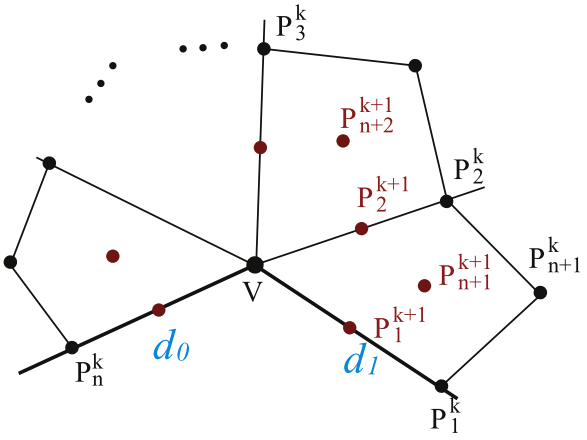

Fig. 8. The boundary rules for the NUISS scheme.

1. Because P_i^k only influences one direction, so we first compute D_i^k such that the limit position of non-uniform cubic B-spline for control polygon P_{i+n}^k, D_i^k and P_{i-1+n}^k with the knot intervals $d_{0,i-1}$, $d_{0,i-1}$, $d_{0,i+1}$, $d_{0,i+1}$ is P_i^k,

$$D_i^k = \frac{(2d_{0,i+1}+d_{0,i-1})(2d_{0,i-1}+d_{0,i+1})}{6d_{0,i-1}d_{0,i+1}}P_i^k - \frac{d_{0,i-1}(2d_{0,i-1}+d_{0,i+1})}{6d_{0,i+1}(d_{0,i-1}+d_{0,i+1})}P_{i+n}^k - \frac{d_{0,i+1}(2d_{0,i+1}+d_{0,i-1})}{6d_{0,i-1}(d_{0,i-1}+d_{0,i+1})}P_{i+n-1}^k.$$

2. Compute C such that

$$P_0^k = \left(1-\sum_{i=1}^{n}(m_i+f_i)\right)C + \sum_{i=1}^{n} m_i D_i^k + f_i P_{i+n}^k. \tag{5}$$

Thus, we can solve C as the linear combination of P_0^k, D_i^k and P_{i+n}^k;

$$C = \frac{P_0^k - (\sum_{i=1}^{n} m_i D_i^k + f_i P_{i+n}^k)}{1-\sum_{i=1}^{n}(m_i+f_i)}, \tag{6}$$

where m_i and f_i are defined in Section 4.1.

3. Compute the contribution for the ith face point P_{i+n}^{k+1} as the weighted average of all the vertices of that face using the face point rule in [36]:

$$P_{i+n}^{k+1} = \frac{\omega_0 C + \omega_1 D_i^k + \omega_3 D_{i+1}^k + \omega_2 P_{i+n}^k}{l_i \sum_{j=0}^{3}\omega_j},$$

where $\omega_0 = 9d_{0,i}d_{0,i+1}$, $\omega_1 = 3d_{0,i+1}(d_{0,i-2}+d_{0,i+2}+d_{0,i})$, $\omega_2 = (d_{0,i-2}+d_{0,i+2}+d_{0,i})(d_{0,i-1}+d_{0,i+3}+d_{0,i+1})$, $\omega_3 = 3d_{0,i}(d_{0,i-1}+d_{0,i+3}+d_{0,i+1})$ and l_i is the valence of the ith face.

4. The contribution for the edge point P_i^{k+1} is the linear combinations of C, D_i^k, D_{i-1}^k, D_{i+1}^k, P_{i+n-1}^k and $P_{i,n}^k$ using the edge point rule in [36],

$$P_i^{k+1} = \frac{f_1(e_0 D_{i-1}^k + e_1 C + e_2 D_{i+1}^k)}{2(f_1+f_2)(e_0+e_1+e_2)} + \frac{f_2(e_0 P_{i+n-1}^k + e_1 D_i^k + e_2 P_{i+n}^k)}{2(f_1+f_2)(e_0+e_1+e_2)},$$

where $e_0 = (2d_{0,i-1}+d_{0,i+1})d_{0,i+1}$, $e_1 = 6(d_{0,i-1}+d_{0,i+1})d_{0,i-1}d_{0,i+1}$, $e_2 = (2d_{0,i+1}+d_{0,i-1})d_{0,i-1}$, $f_1 = 3d_{0,i}$ and $f_2 = d_{0,i-2}+d_{0,i}+d_{0,i+2}$.

4.3. Boundary rules

We now generalize the rules in the last section to handle boundaries referring to Fig. 8. Suppose VP_1^k and VP_n^k are two boundary edges and the other vertices are shown in Fig. 8. In the following, we give the details to compute the contribution to the neighbor face points or edge points from vertex V. These rules are similar as the interior rules except the way to compute point C and the boundary edge contributions, which are the following steps:

1. Compute D_i^k for $i = 2, \ldots, n$ for each P_i^k with the same formula as that in last section;

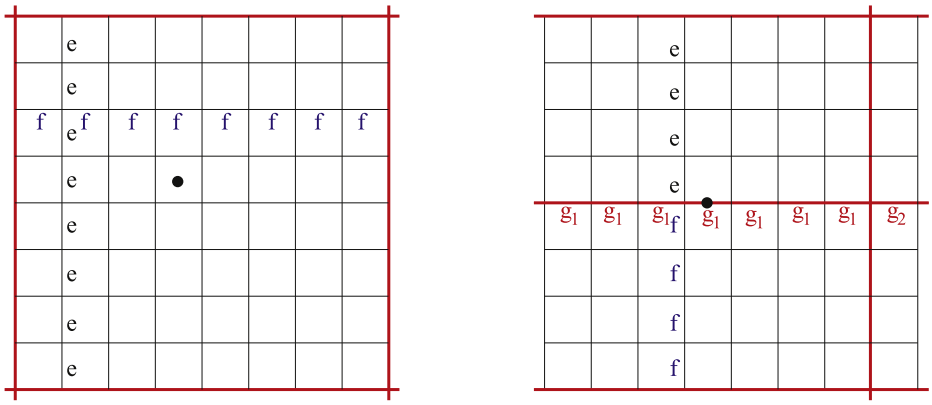

Fig. 9. Knot intervals after refinement.

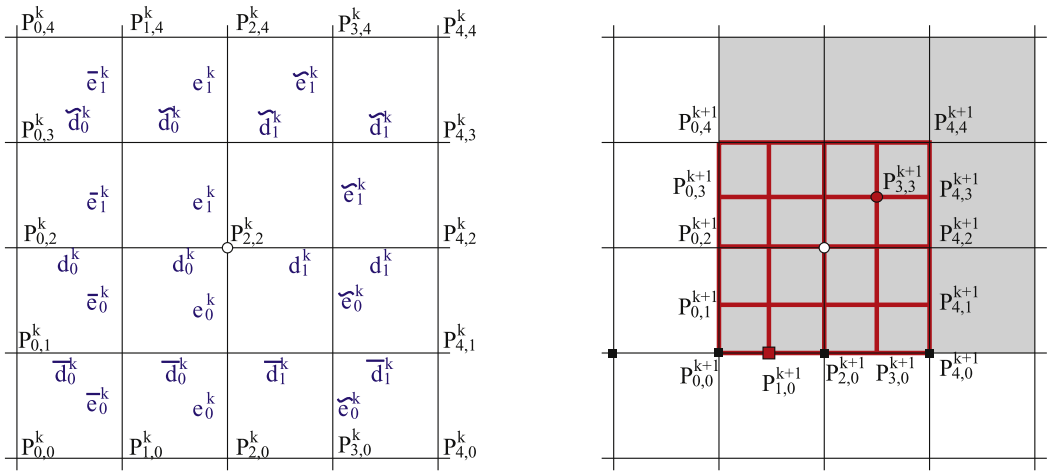

Fig. 10. Notations for the mask for a regular vertex.

2. Compute $C = \frac{(2d_0+d_1)(2d_1+d_0)}{6d_0d_1}V - \frac{d_1(2d_1+d_0)}{6d_0(d_0+d_1)}P_n^k + \frac{d_0(2d_0+d_1)}{6d_1(d_0+d_1)}P_1^k$;
3. Compute the contribution for the face points P_{i+n}^{k+1} using the boundary face points rules by linear combination of C, D_i^k, P_1^k and P_n^k;
4. Compute the contribution for the edge points P_i^{k+1} using the boundary edge points rules by linear combination of C, D_i^k, P_1^k and P_n^k.

Remark 1. We can see that the boundary rule is designed such that the boundary curves interpolate the boundary control points using non-uniform four-point subdivision curve scheme. Thus, the final boundary curves are C^1 continuity which interpolate the boundary control points. The examples with boundaries are shown in Figs. 13 and 17. And we can very easily to generalize our scheme to support sharp features using the similar approaches in [51,52].

4.4. Continuity analysis

In this section, we analyze the convergence and smoothness properties of NUISS limit surface. In particular, we prove that NUISS generates a C^1-continuous limit surface independently of the initial parameters configuration except being G^1 at the extraordinary points, which is verified by some numerical experimentations.

For the sake of simplicity, we consider the surface after one subdivision step when all faces are quadrilaterals. In the initial mesh $\mathbf{M}^0$, the vertices of the mesh $\mathbf{M}^0$ are denoted as $\mathbf{V}$, the edges correspond to the limit of a set of curves, which are denoted by $\mathbf{E}$ and the faces correspond to the limit of a set of patches, which are denoted by $\mathbf{F}$.

Lemma 1. *For any point inside of* $\mathbf{F}$, *NUISS rule generates a* C^1*-continuous limit surface at the point.*

Proof. Referring to Fig. 9a, after several levels of refinement, for all the edges in the interior of the face, each row of edges have the same knot intervals, and each column of edges have the same knot intervals. Although the knot intervals may

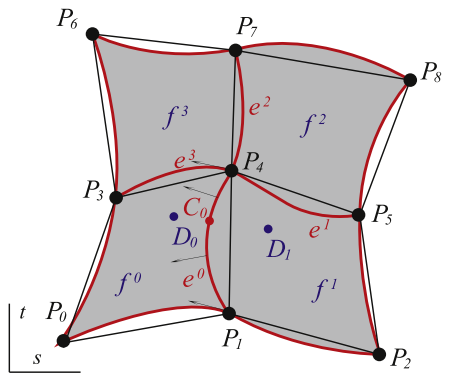

Fig. 11. Notations for the continuous proof at a regular vertex.

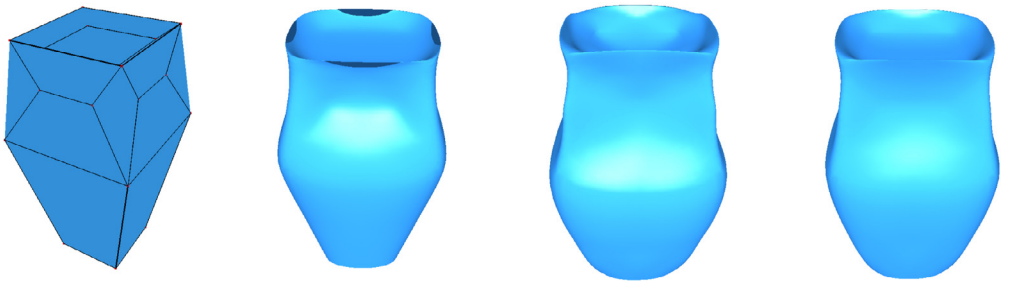

Fig. 12. Subdivision surfaces with different parametrization methods. Figures (from left to right) are the initial control grid, the interpolation subdivision surface with uniform, chordal and centripetal parametrization, respectively.

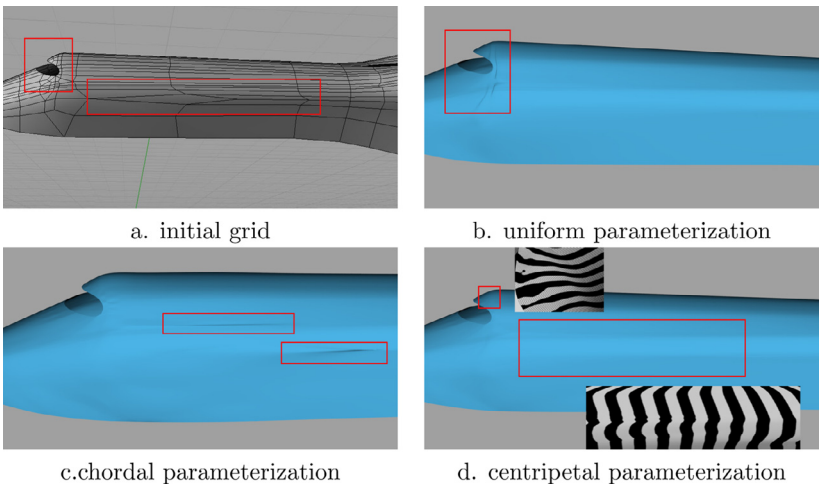

Fig. 13. Subdivision surfaces with different parametrization methods.

be different for different rows or columns, but we can see that the scheme is invariant if we scale the whole rows or columns of knot intervals. Thus, for any such point, the situation can be regarded as a tensor-product of uniform four-point interpolatory subdivision, which means the limit surface is C^1 at any point in **F**. □

Lemma 2. *For any point inside of* **E**, *NUISS rule generates a* C^1*-continuous limit surface at the point.*

Proof. Referring to Fig. 9b, after several levels of refinement, for all the edges in the interior of the two adjacent two faces, each column of edges inside each face have the same knot intervals. Thus, for any point inside an edge in **E**, the situation can be regarded as a non-uniform four-point interpolatory curve subdivision, which means the limit surface is also C^1 at these points. □

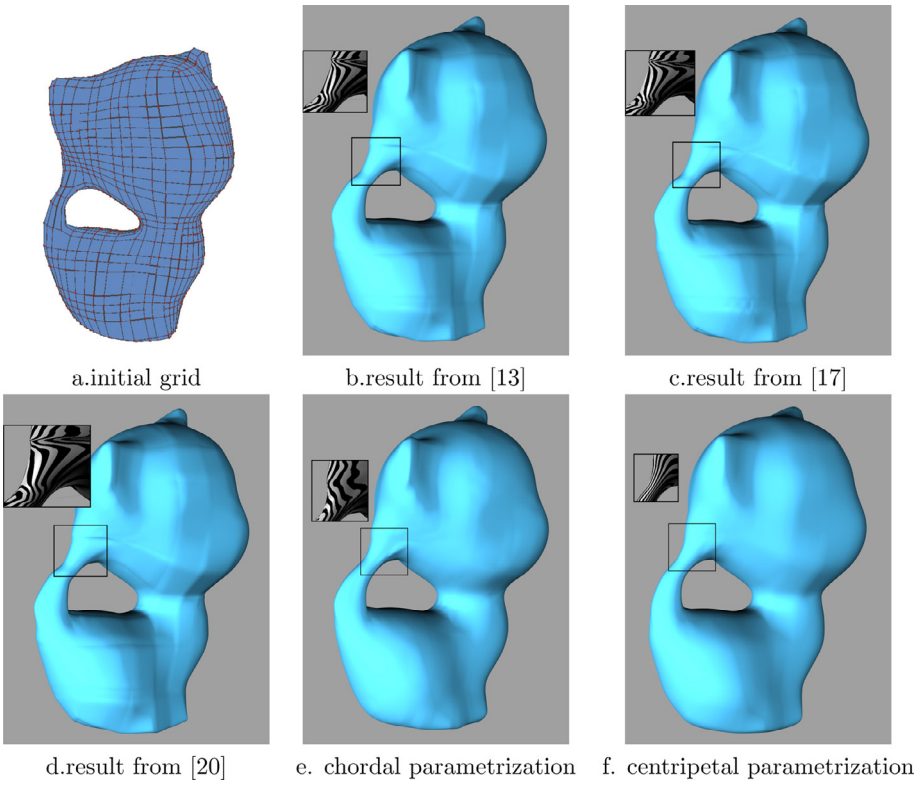

Fig. 14. Subdivision surfaces with different parametrization methods. Figure a is the initial control grid, figures b, c, and d are the limit surfaces for three uniform interpolation subdivision surfaces of [13], [17] and [20], figures e and f are the limit surfaces of non-uniform subdivision with chordal and centripetal parametrization.

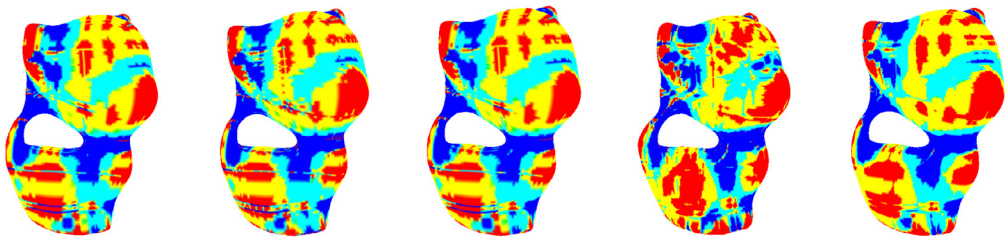

Fig. 15. The Gaussian curvature plots for the subdivision limit surfaces with different parametrization methods, which are the results from [13,17,20], non-uniform subdivision with chordal and centripetal parametrization respectively.

In the following, we will prove that the limit surface is also C^1 at all the regular points in $\mathbf{V}$. For simplicity, we assume the two neighbor of points $P^0_{i,j}, 0 \le i, j \le 4$ around $P^0_{2,2}$ are all regular because we must encounter the situation after two levels of subdivision. The associated knot intervals are d^0_i, $\widetilde{d}^0_i$, $\overline{d}^0_i$, and e^0_i, $\widetilde{e}^0_i$, $\overline{e}^0_i, i = 0, 1$ respectively. After k level subdivision, the the two neighbor of points $P^k_{i,j}, 0 \le i, j \le 4$ and the associated knot intervals are d^k_i, $\widetilde{d}^k_i$, $\overline{d}^k_i$, and e^k_i, $\widetilde{e}^k_i$, $\overline{e}^k_i, i = 0, 1$ respectively. According to the knot intervals refinement rule,

$$d^k_i = d^0_i \quad \widetilde{d}^k_i = \frac{d^{k-1}_i + \widetilde{d}^{k-1}_i}{2}, \quad \overline{d}^k_i = \frac{d^{k-1}_i + \overline{d}^{k-1}_i}{2};$$
$$e^k_i = e^0_i \quad \widetilde{e}^k_i = \frac{e^{k-1}_i + \widetilde{e}^{k-1}_i}{2}, \quad \overline{e}^k_i = \frac{e^{k-1}_i + \overline{e}^{k-1}_i}{2}.$$

Lemma 3. *There exists a constant A independent of k such that $|\widetilde{d}^k_i - d^k_i|, |\overline{d}^k_i - d^k_i| \le A2^{-k}$ and $|\widetilde{e}^k_i - e^k_i|, |\overline{e}^k_i - e^k_i| \le A2^{-k}$.*

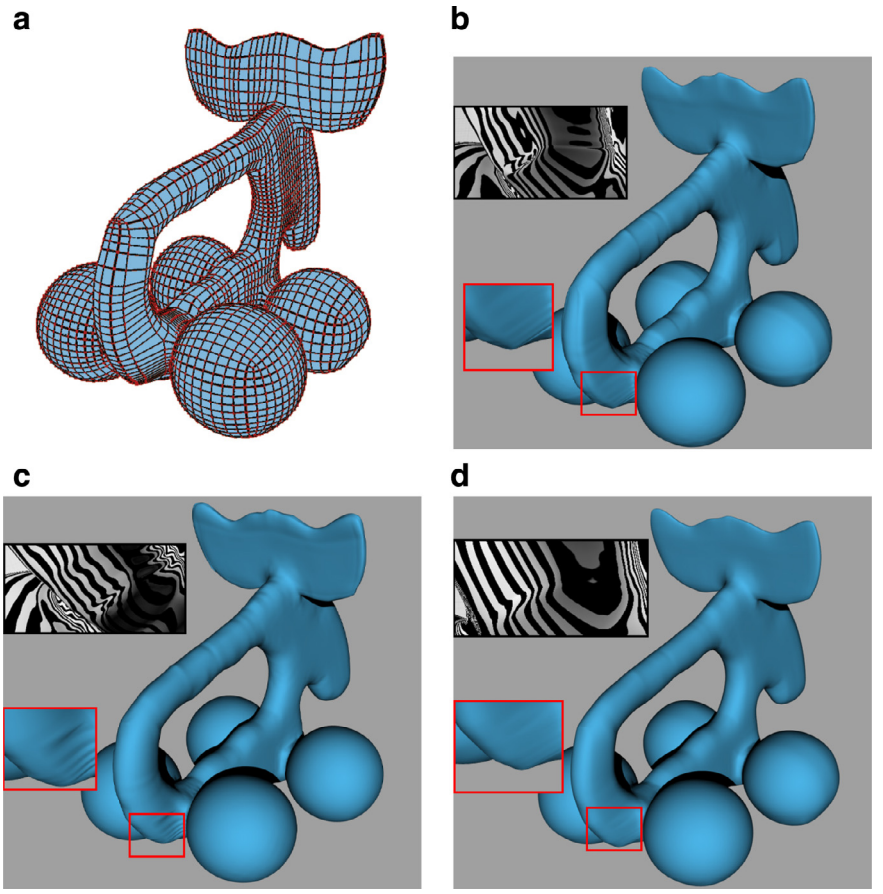

Fig. 16. Subdivision surfaces with different parametrization methods. Figures (b), (c), and (d) are the NUISSes with uniform, chordal and centripetal parametrization. The highlights of the shape and the reflection lines for the red rectangle region are also shown in the figures.

Proof. According to the knot interval refinement rule,

$$\widetilde{d}_i^k - d_i^k = \frac{\widetilde{d}_i^{k-1} - d_i^{k-1}}{2} = \frac{\widetilde{d}_i^0 - d_i^0}{2^k}. \tag{7}$$

Thus $|\widetilde{d}_i^k - d_i^k| \le A2^{-k}$ if $A > |\widetilde{d}_i^0 - d_i^0|$. Similarly, we can prove the other inequations. □

Lemma 4. *For any constant C_1, C_2, $C_3 \in R$, there exists a generic constant A_1 independent of k, such that*

$$|\varphi_i(d_0, d_1, d_2) - \varphi_i(d_0 + C_1 2^{-k}, d_1 + C_2 2^{-k}, d_2 + C_3 2^{-k})| \le A_1 2^{-k}. \tag{8}$$

Proof. See the Lemma 2 in [50] for more details of the proof. □

Now we can define two local subdivision matrixes M^k and M, where the matrix M^k is the local NUISS subdivision matrix between the points $P_{i,j}^k$ and $P_{i,j}^{k+1}$ using the knot interval $\widetilde{d}_i^k$, $\overline{d}_i^k$, d_i^k and $\widetilde{e}_i^k$, $\overline{e}_i^k$, e_i^k. And the matrix M is the subdivision matrix for the same grid when the knot intervals $\widetilde{d}_i^k = \overline{d}_i^k = d_i^k$ and $\widetilde{e}_i^k = \overline{e}_i^k = e_i^k$ for $i = 0, 1$. According to [50], the subdivision rule defined by local matrix M is C^1. Thus, in order to prove NUISS is C^1 at $P_{2,2}^0 \in \mathbf{V}$, we first prove that NUISS is C^0 at $P_{2,2}^0$ via proving the matrix M^k is asymptotically equivalent to matrix M. And then, we prove NUISS is C^1 at $P_{2,2}^0$ in Theorem 1.

Lemma 5. *At any point $P_{2,2}^0 \in \mathbf{V}$ of valence 4, the local matrix operator M^k of NUISS is asymptotically equivalent to the local matrix operator M.*

Proof. The local matrix operators M^k and M are asymptotically equivalent if $\sum_{k=0}^{\infty} ||M^k - M||_\infty < \infty$ [53] (Fig. 10). Being $||M^k - M||_\infty = \max_i \sum_j |M_{i,j}^k - M_{i,j}|$, we prove that

$$\sum_j |M_{i,j}^k - M_{i,j}| \le A2^{-k}, \forall i, \tag{9}$$

with A a generic constant independent of k.

In the following, we focus our attention on the rows of M^k and M corresponding to edge and face points and show that relation (9) holds for each of them.

- Edge points:
  The edge point computation of NUISS is actually a non-uniform curve subdivision rule. For example, the edge point $P^{k+1}_{1,0}$ is a linear combination of $P^k_{i,1}, i = 0, \ldots, 3$ with local knot intervals $\bar{d}^k_0$ and $\bar{d}^k_1$.

$$P^{k+1}_{1,0} = \sum_{i=0}^{3} P^k_{i,1}\phi_i(\bar{d}^k_0, \bar{d}^k_0, \bar{d}^k_1); \tag{10}$$

  According to the equations (17–19) in [50], we can prove that Eq. (9) holds for all the neighbor edge points.
- Face Points:
  The face point computation of NUISS is actually a linear combination of the neighbor 4×4 control points. For example, for face point $P^{k+1}_{3,3}$ in M^k is a linear combination of all $P^k_{i,j}, i, j = 1, \ldots, 4$.

$$P^{k+1}_{3,3} = \sum_{i=1}^{4}\sum_{j=1}^{4} P^k_{i,j}\psi_{i,j}, \tag{11}$$

  where

$$\psi_{i,j} = \frac{\varphi_{i-1}(d^k)\varphi_{j-1}(e^k) + \varphi_{4-i}(D^k)\varphi_{j-1}(\widetilde{e}^k) + \varphi_{i-1}(\widetilde{d}^k)\varphi_{4-j}(E^k) + \varphi_{4-i}(\widetilde{D}^k)\varphi_{4-j}(\widetilde{E}^k)}{4},$$

  and $d^k = [d^k_0, d^k_1, d^k_1]$, $D^k = [d^k_1, d^k_1, d^k_0]$, $\widetilde{d}^k = [\widetilde{d}^k_0, \widetilde{d}^k_1, \widetilde{d}^k_1]$, $\widetilde{D}^k = [\widetilde{d}^k_1, \widetilde{d}^k_1, \widetilde{d}^k_0]$, $e^k = [e^k_0, e^k_1, e^k_1]$, $E^k = [e^k_1, e^k_1, e^k_0]$, $\widetilde{e}^k = [\widetilde{e}^k_0, \widetilde{e}^k_1, \widetilde{e}^k_1]$, $\widetilde{E}^k = [\widetilde{e}^k_1, \widetilde{e}^k_1, \widetilde{e}^k_0]$.
  Similarly, the face point $\widehat{P}^{k+1}_{3,3}$ in M can be computed via the following equation

$$\widehat{P}^{k+1}_{3,3} = \sum_{i=1}^{4}\sum_{j=1}^{4} P^k_{i,j}\widehat{\psi}_{i,j}, \tag{12}$$

  where

$$\widehat{\psi}_{i,j} = \frac{\varphi_{i-1}(d^k)\varphi_{j-1}(e^k) + \varphi_{4-i}(D^k)\varphi_{j-1}(e^k) + \varphi_{i-1}(d^k)\varphi_{4-j}(E^k) + \varphi_{4-i}(D^k)\varphi_{4-j}(E^k)}{4}.$$

  Thus,

$$\begin{aligned}\sum_{i,j}|\psi_{i,j} - \widehat{\psi}_{i,j}| &= \frac{1}{4}\sum_{i,j}(|\varphi_{4-i}(D^k)(\varphi_{j-1}(\widetilde{e}^k) - \varphi_{j-1}(e^k)) + \varphi_{4-j}(E^k)(\varphi_{i-1}(\widetilde{d}^k) - \varphi_{i-1}(d^k))\\ &\quad + \varphi_{4-i}(D^k)(\varphi_{4-j}(\widetilde{E}^k) - \varphi_{4-j}(E^k)) + \varphi_{4-j}(\widetilde{E}^k)(\varphi_{4-i}(\widetilde{D}^k) - \varphi_{4-i}(D^k))|)\\ &\le A_1 2^{-k}\sum_{i,j}\frac{|\varphi_{4-i}(D^k)| + |\varphi_{4-j}(E^k)| + |\varphi_{4-i}(D^k)| + |\varphi_{4-j}(\widetilde{E}^k)|}{4}\\ &\le A_2 2^{-k}.\end{aligned}$$

  The first inequality follows from Lemmas 3 and 4. Thus, the Eq. (9) also holds for all the face points.

□

The previous result naturally implies the following theorem.

Theorem 1. *NUISS generates C^1-continuous limit surfaces except at those extraordinary points.*

Proof. We prove that the theorem based on Lemma 5 and the notations illustrated in Fig. 11. Given a regular vertex P_4 with the surrounding vertices P_j. The four edges connected with P_4 correspond to the limit of four subdivision curves $e^i, i = 0, \ldots, 3$ and the four faces correspond to the limit of four patches $f^i, i = 0, \ldots, 3$. Then for any point inside the patch as already observed above, C^1 smoothness of the limit surface is trivially established according to Lemma 1. Thus we can define f^0_s and f^1_s to be the one directional derivative. Also, for any point in the interior of the curves in **E**, the limit surface is also C^1 according to Lemma 2, i.e, f^0 and f^1 is C^1 at any point C_0 in the interior of the curve e^0,

$$f^0_s(C_0) = f^1_s(C_0). \tag{13}$$

Now, we prove that the final subdivision limit surface is also C^1 at point P_4. Actually, according to Lemma 5, $f^0_s(C_0)$ and $f^1_s(C_0)$ is at least C^0 for all the points in the curve e^0 (including two boundary points), which implies that

$$f^0_s(P_4) = \lim_{C_0 \to P_4} f^0_s(C_0), \quad f^1_s(P_4) = \lim_{C_0 \to P_4} f^1_s(C_0). \tag{14}$$

Table 1
Maximum angle in radian at an specified point with valence 3 to 8 for the interpolatory subdivision continuity test.

level	$n = 3$	$n = 4$	$n = 5$	$n = 6$	$n = 7$	$n = 8$
1	1.397159	1.031612	1.039907	1.204761	1.161872	1.316257
5	0.482394	0.221278	0.230938	0.244731	0.219948	0.220254
9	0.077129	0.020339	0.019371	0.016961	0.015217	0.013168
13	0.016947	0.003076	0.002358	0.002176	0.001628	0.001418
15	0.006671	0.000912	0.000631	0.000483	0.000370	0.000310

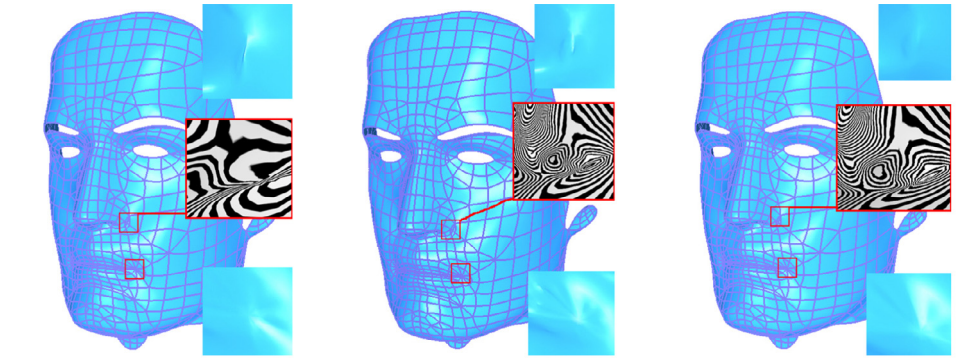

Fig. 17. Subdivision surfaces with different parametrization methods on the model with both triangle and quadrangle faces. Figures (b), (c), and (d) are the NUISSes with uniform, chordal and centripetal parametrization.

Combining the above two equations, we can get

$$f_s^0(P_4) = \lim_{C_0 \to P_4} f_s^0(C_0) = \lim_{C_0 \to P_4} f_s^1(C_0) = f_s^1(P_4). \tag{15}$$

Thus, f^0 and f^1 are C^1 smoothness at point P_4. Similarly, we can prove the other patches are also C^1 at point P^4, which completes the proof. □

Now, we only need to investigate the continuity at the extraordinary vertices. Because the subdivision matrix has no symmetries except the uniform case, so it is difficult to perform the Eigen-analysis for extraordinary points. Being analogous to [36,37,39,40], we assume that the continuity is only associated with the knot interval configurations. So we provide a numerical test on a typical example for which all the z-coordinates are zeros except one valence n vertex is one. For the same geometry, we test the continuity for 10^5 different knot intervals configurations. For each test, the knot intervals for the neighbor edges are set to be a random value from 1 to 100. The reason to choose the range being 100 is because we believe this value is good enough for the real applications. Also we do not study valences greater than eight because high valence extraordinary points are rarely used in practice. We measure the maximum angle between the n normals of the planes defined by the vertex and the neighbor edge points and test how fast the neighboring faces of the considered vertex become coplanar. All our experimentations show that the limit surfaces are G^1 at the extraordinary points. Table 1 shows the corresponding maximum angles with one knot interval is 5 and the others are 1 for a valence 3 to 8 vertex.

5. Numerical examples

We conclude by presenting some numerical experimentation in order to show the quality of NUISS limit surfaces and compare them with three uniform interpolation subdivision methods in [13,17,20].

We start with a simple example in Fig. 12. To produce the models, we create a mesh model with several extraordinary points whose section poly-lines have corresponding edges of different lengths. In such situation, the uniform parameterization introduces self-intersection. And the chordal parameterization introduces a significant distortion, while centripetal parameterization produces very good result as shown in Fig. 12.

Now we show more examples of our NUISS limit surfaces on some real-world models. The first one is an aircraft model, which is composed with the head and the body. The head has very dense mesh and the body has very long section edges, which makes the model to be a significantly non-uniform mesh. Thus, in the head of the aircraft, the uniform parameterization leads cusps and self-intersections and the chordal parametrization gives cusps in the body part. While the centripetal parameterization produces very reasonable shape to interpolate the initial control grid.

Actually, most real-world models have very good quality mesh without significantly different edge lengths, such as the following kitty model (Fig. 14). We compare the subdivision surfaces with three different uniform subdivision schemes

[13,17,20] and the non-uniform subdivision schemes for chordal and centripetal parametrizations. The three uniform subdivision schemes produce very similar poor quality limit surfaces, while the limit surfaces with non-uniform parameterization produce much better results. And we can see that the non-uniform subdivision surface with centripetal parametrization has much better reflection lines than that of chordal parameterization. The Gaussian curvature plots in Fig. 15 also show the same behavior.

The second model is an elk model. Same as the kitty model, the elk model does not have significantly different edge lengthes. Fig. 16 shows the NUISS limit surfaces produced by different parametrization methods. For uniform parametrization, the surface leads very poor quality shape as shown in Fig. 16b. On the other hand, the chordal parametrization scheme leads to better shape but still not satisfactory (Figure 16c). The limit surface with centripetal parametrization scheme produces very good limit surface as shown in Fig. 16d.

The last example is a mask model which has both triangle and quadrangle faces. The model is also almost uniform except in some feature regions such as the nose and mouth. As shown in Fig. 17, we can see that the NUISS limit surface with centripetal parameterization can produce more fair and smoother shape than those for both uniform and chordal parameterization methods.

6. Summary and future work

The paper presents an observation on the non-uniform four-point interpolatory subdivision and non-uniform cubic B-spline curve refinement rules. The observation is that the non-uniform four-point interpolatory subdivision scheme can be derived as an average of two spline segments using the local knot intervals. A heuristic is thus derived from the observation, which allows to construct non-uniform interpolatory subdivision schemes from non-uniform approximating subdivision schemes. Based on the observation, we present a novel non-uniform interpolatory subdivision surface scheme that generalizes well-known non-uniform interpolatory four-point schemes to arbitrary topology meshes. Lots of numerical examples show that the interpolatory subdivision limit surface with centripetal parameterization generates best shapes compared with those for uniform and chord parameterization. This behavior has been well established in the univariate case both with numerical examples and theoretical proof [46,47,54,55]. Our future objective is the generalization the theoretical proof for univariate four-point subdivision scheme to our non-uniform interpolatory subdivision scheme at the extraordinary points.

Acknowledgements

The authors are supported by the NSF of China (Grant nos. 11031007, 60903148, 11371341), a NKBRPC (Grant no. 2011CB302400), the Fundamental Research Funds for the Central Universities, SRF for ROCS SE, and the Youth Innovation Promotion Association CAS.

References

[1] J. Warren, H. Weimer, Subdivision Methods for Geometric Design, Morgan Kaufmann, 2002.
[2] D. Doo, M. Sabin, Behaviour of recursive division surfaces near extraordinary points, Comput. Aided Des. 10 (1978) 356–360.
[3] E. Catmull, J. Clark, Recursively generated B-spline surfaces on arbitrary topological meshes, Comput. Aided Des. 10 (1978) 350–355.
[4] C. Loop, Smooth subdivision surfaces based on triangles, University of Utah, 1987 (Master's thesis).
[5] L. Kobbelt, $\sqrt{3}$-subdivision, in: SIGGRAPH '00: Proceedings of the Twenty-Seventh Annual Conference on Computer Graphics and Interactive Techniques, ACM Press/Addison-Wesley Publishing Co., 2000, pp. 103–112.
[6] L. Velho, D. Zorin, Quasi 4–8 subdivision, Comput. Aided Geom. Des. 18 (2001) 345–358.
[7] L. Velho, D. Zorin, 4–8 subdivision, Comput. Aided Geom. Des. 18 (2001) 397–427.
[8] J. Stam, C. Loop, Quad/Triangle subdivision, Comput. Graph. Forum 22 (2003) 1–7.
[9] J. Peters, L. Shiue, Combining 4- and 3-direction subdivision, ACM Trans. Graph. 23 (2004) 980–1003.
[10] N. Dyn, D. Levin, J.A. Gregory, A four-point interpolatory subdivision scheme for curve design, Comput. Aided Geom. Des. 4 (1987) 257–268.
[11] N. Dyn, D. Levin, A butterfly subdivision scheme for surface interpolation with tension control, ACM Trans. Graph. 9 (1990) 160–169.
[12] D. Zorin, P. Schröder, W. Sweldens, Interpolating Subdivision for meshes with arbitrary topology, in: SIGGRAPH '96: Proceedings of the Twenty-Third Annual Conference on Computer Graphics and Interactive Techniques, ACM, New York, NY, USA, 1996, pp. 189–192.
[13] L. Kobbelt, Interpolatory subdivision on open quadrilateral nets with arbitrary topology, Comput. Graph. Forum 15 (1996) 400–410.
[14] C. Deng, W. Ma, A unified interpolatory subdivision scheme for quadrilateral meshes, ACM Trans. Graph. 32(3) (2013) 1–11.
[15] U. Labsik, G. Greiner, Interpolatory $\sqrt{3}$ subdivision, Comput. Graph. Forum 19 (2000) 131–138.
[16] G. Li, W. Ma, H. Bao, Interpolatory $\sqrt{2}$-subdivision surfaces, in: Proceedings of the Geometric Modeling and Processing, 2004, pp. 185–194.
[17] S. Lin, F. You, X. Luo, Z. Li, Deducing interpolating subdivision schemes from approximating subdivision schemes, in: SIGGRAPH Asia '08: ACM SIGGRAPH Asia Papers, ACM, New York, NY, USA, 2008, pp. 1–7.
[18] J. Maillot, J. Stam, A unified subdivision scheme for polygonal modeling, Comput. Graph. Forum 20 (2001) 471–479.
[19] G. Li, W. Ma, A method for constructing interpolatory subdivision schemes and blending subdivisions, Comput. Graph. Forum 26 (2007) 185–201.
[20] X. Li, J. Zheng, An alternative method for constructing interpolatory subdivision from approximating subdivision, Comput. Aided Geom. Des. 29(4) (2012) 474–484.
[21] Z. Luo, W. Qi, On interpolatory subdivision from approximating subdivision scheme, Appl. Math. Comput. 220(1) (2013) 339–349.
[22] L. Romani, From approximating subdivision schemes for exponential splines to high-performance interpolating algorithms, J. Comput. Appl. Math. 224 (2009) 383–396.
[23] C. Conti, L. Gemignani, L. Romani, From symmetric subdivision masks of Hurwitz type to interpolatory subdivision masks, Linear Algebra Appl. 431 (2009) 1971–1987.
[24] C. Beccari, G. Casciola, L. Romani, A unified framework for interpolating and approximating univariate subdivision, Appl. Math. Comput. 216 (2010) 1169–1180.
[25] C. Conti, L. Gemignani, L. Romani, From approximating to interpolatory non-stationary subdivision schemes with the same generation properties, Adv. Comput. Math. 35 (2011) 217–241.

[26] Z. Luo, W. Qi, On interpolatory subdivision from approximating subdivision scheme, Appl. Math. Comput. 220 (2013) 339–349.
[27] R.Q. Jia, Interpolatory subdivision schemes induced by box Splines, Appl. Comput. Harmon. Anal. 8 (2000) 286–292.
[28] C. Conti, L. Gemignani, L. Romani, A constructive algebraic strategy for interpolatory subdivision schemes induced by bivariate box splines, Adv. Comput. Math. 39 (2013) 395–424.
[29] G. Albrechta, L. Romani, Convexity preserving interpolatory subdivision with conic precision, Appl. Math. Comput. 219(8) (2012) 4049–4066.
[30] M. Halstead, M. Kass, T. DeRose, Efficient fair interpolating using Catmull–Clark surfaces, in: SIGGRAPH '93: Proceedings of the Twentieth Annual Conference on Computer Graphics and Interactive Techniques, 1993, pp. 35–44.
[31] J. Zheng, Y. Cai, Making Doo–Sabin surface interpolation always work over irregular meshes, Vis. Comput. 21 (2005) 242–251.
[32] C. Deng, X. Yang, A simple method for interpolating meshes of arbitrary topology by Catmull—Clark surfaces, Vis. Comput. 26(2) (2010) 137–146.
[33] A. Nasri, Polyhedral subdivision methods for free-form surfaces, ACM Trans. Graph. 6 (1987) 29–73.
[34] J. Zheng, Y. Cai, Interpolation over arbitrary topology meshes using a two-phase subdivision scheme, IEEE Trans. Vis. Comput. Graph. 12 (2006) 301–310.
[35] C. Deng, W. Ma, Constructing an interpolatory subdivision scheme from Doo–Sabin subdivision, in: Proceedings of the twelfth International Conference on Computer-Aided Design and Computer Graphics, IEEE, 2013, pp. 215–222.
[36] T. Sederberg, J. Zheng, D. Sewell, M. Sabin, Non-uniform recursive subdivision surfaces, in: SIGGRAPH '98: Proceedings of the Twenty-Fifth Annual Conference on Computer Graphics and Interactive Techniques, ACM Press/Addison-Wesley Publishing Co., 1998, pp. 387–394.
[37] K. Muller, L. Reusche, D. Fellner, Extended subdivision surfaces: building a bridge between NURBS and Catmull-Clark surfaces, ACM Trans. Graph. 25 (2006) 268–292.
[38] T.J. Cashman, U.H. Augsdörfer, N.A. Dodgson, M.A. Sabin, NURBS with extraordinary points: high-degree, non-uniform, rational subdivision schemes, ACM Trans. Graph. 28 (3) (2009) 1–9.
[39] K. Muller, C. Funfzig, L. Reusche, D. Hansford, G. Farin, H. Hagen, DINUS-Double insertion, non-uniform, stationary subdivision surfaces, ACM Trans. Graph. 29 (2010) 1–21.
[40] Z. Huang, G. Wang, Non-uniform recursive Doo–Sabin surfaces, Comput. aided Des. 43 (2013) 1527–1533.
[41] X. Li, J. Zheng, T.W. Sederberg, T.J.R. Hughes, M.A. Scott, On the linear independence of T-splines blending functions, Comput. Aided Geom. Des. 29 (2012) 63–76.
[42] A. Riffnaller-Schiefer, U. Augsdorfera, D. Fellner, Isogeometric shell analysis with NURBS compatible subdivision surfaces, Appl. Math. Comput. 272(1) (2016) 139–147.
[43] X. Li, T. Finnigin, T.W. Sederberg, G^1 non-uniform Catmull–Clark surfaces, ACM Trans. Graph. (SIGGRAPH 2016) 35(4) (2016).
[44] E. Lee, Choosing nodes in parametric curve interpolation, Comput. Aided Des. 21 (1989) 363–370.
[45] E. Kuznetsov, A. Yu, Yakimovich, The best parameterization for parametric interpolation, J. Comput. Appl. Math. 191 (2006) 239–245.
[46] I. Daubechies, I. Guskov, W. Sweldens, Regularity of irregular subdivision, Constr. Approx. 15 (1999) 381–426.
[47] N. Dyn, M.S. Floater, K. Hormann, Four-point curve subdivision based on iterated chordal and centripetal parameterizations, Comput. Aided Geom. Des. 26 (2009) 279–286.
[48] C. Beccari, G. Casciola, L. Romani, Non-uniform interpolatory curve subdivision with edge parameters built upon compactly supported fundamental splines, BIT Numer. Math. 51 (2011) 781–808.
[49] C. Beccari, G. Casciola, L. Romani, Polynomial-based non-uniform interpolatory subdivision with features control, J. Comput. Appl. Math. 235 (2011) 4754–4769.
[50] C.V. Beccari, G. Casciola, L. Romani, Non-uniform non-tensor product local interpolatory subdivision surfaces, Comput. Aided Geom. Des. 30 (2013) 357–373.
[51] T. DeRose, M. Kass, T. Truong, Subdivision surfaces in character animation, in: Proceedings of the Twenty-Fifth Annual Conference on Computer Graphics and Interactive Techniques, in: SIGGRAPH '98, ACM, New York, NY, USA, 1998, pp. 85–94.
[52] J. Kosinka, M.A. Sabin, N.A. Dodgson, Semi-sharp creases on subdivision curves and surfaces, Comput. Graph. Forum 33 (5) (2014) 217–226.
[53] N. Dyn, D. Levin, Analysis of asymptotically equivalent binary subdivision schemes, J. Math. Anal. Appl. 193 (1995) 594–621.
[54] M. Floater, On the deviation of a parametric cubic spline interpolant from its data polygon, Comp. Aided Geom. Des. 25 (2008) 148–156.
[55] C. Yuksel, S. Schaefer, J. Keyser, On the parameterization of Catmull–Rom curves, in: Proceedings of the ACM Joint Conference on Geometric and Physical Modeling, ACM, 2009, pp. 47–53.